Sorption properties of activated carbons for the capture of methyl iodide in the context of nuclear industry

M. Chebbi, C. Monsanglant-Louvet, P. Parent, Claire Gerente, Laurence Le Coq, B.M. Mokili

Carbon Trends 7 (2022) 100164

Contents lists available at ScienceDirect

Carbon Trends

journal homepage: www.elsevier.com/locate/cartre

Sorption properties of activated carbons for the capture of methyl iodide in the context of nuclear industry

M. Chebbi[a,*], C. Monsanglant-Louvet[a], P. Parent[b], C. Gerente[c], L. Le Coq[c], B.M. Mokili[d]

[a] Institut De Radioprotection Et De Sûreté Nucléaire (IRSN), PSN-RES Saclay, Gif-sur-Yvette 91192 France
[b] CNRS, Aix Marseille University, CINaM, Marseille, France
[c] IMT Atlantique, GEPEA UMR CNRS 6144, Nantes F-44307, France
[d] CNRS/IN2P3, Subatech UMR 6457, IMT Atlantique, Université De Nantes, Nantes F-44307 France

ARTICLE INFO

Article history:
Received 21 January 2022
Revised 4 February 2022
Accepted 7 February 2022

Keywords:
TEDA
Activated carbons
XPS
Adsorption isotherm
LDF model

ABSTRACT

In the present study, some commercially available activated carbons were evaluated towards the methyl iodide (CH_3I) capture in the context of nuclear industry. A specific methodology was implemented in order to establish structure-activity relationships between adsorbent characteristics and its adsorption behavior towards CH_3I. On the one hand, the investigated adsorbents were characterized by a combination of physico-chemical techniques. On the other hand, CH_3I retention performance from batch sorption tests under different conditions (temperature and relative humidity) was studied using an original experimental setup. In this work, two conditions were investigated: (i) T = 35°C, R.H. = 26 % ([H_2O] ~15,000 ppmv); (ii) T = 75°C, R.H. = 30 % ([H_2O] ~130,000 ppmv). Different trends were obtained depending on the investigated scenario. At ambient conditions (i), CH_3I adsorption performance was affected after KI/TEDA impregnation because of partial pore blockage phenomena induced by the ~~of~~ impregnants presence within the microporosity. However, TEDA impregnation was found to be required to enhance the trapping stability and to capture CH_3I with superior efficiency at higher temperature (ii).

1. Introduction

The efficient capture of radioiodine potentially released from nuclear facilities in all scenarios (from normal operating conditions to severe accident situations) remains a very major issue to improve nuclear safety and therefore the public acceptability towards the nuclear energy. The particular interest on iodine stands from the high radiological impact of its isotopes (mainly ^{131}I and ^{129}I) at both short and long terms, and the ability of this element to exist as volatile species (such as I_2 and CH_3I) [1–3]. Activated carbons (AC) have been widely used within the ventilation networks of nuclear facilities to prevent from the volatile molecules dissemination to the environment [4–6]. These adsorbents are characterized by a relatively significant contribution from micropores (d < 2 nm), promoting therefore the capture of CH_3I (kinetic diameter of 0.5 – 0.6 nm [7]) by physisorption interactions. However, a drastic decline of retention performance can be expected especially due to the competition for adsorption sites between water vapor (present in large excess in the nuclear field) and CH_3I as a comparison with dry or moderately humid atmospheres. Thus, the nuclear grade activated carbons are commonly co-impregnated with potassium iodide (KI) and triethylendiamine (TEDA), in order to overcome the detrimental humidity effect [8]. TEDA reacts with CH_3I through a chemical reaction leading to a stronger fixation. This reactivity was reported to be dependent on the relative humidity [9]. For a totally dry atmosphere, the chemisorption of CH_3I is governed by an alkylation mechanism based on the S_N2 reaction [10,11]. In humid conditions, CH_3I adsorption is considered to be driven by a protonation mechanism according to recent Density Functional Theory (DFT) calculations [12]. However, the KI impregnation seems to be responsible for an isotopic exchange reaction between the radioactive gaseous iodine species and the stable iodine on the adsorbent phase [8,13,14].

Despite the massive use of these adsorbents in the nuclear field, a poor knowledge exists about the most influencing parameters of activated carbons on CH_3I retention efficiency under different conditions.

The present work aims to investigate the ability of well-characterized commercial activated carbons to trap CH_3I under different conditions (temperature and relative humidity). In the first

* Corresponding author.
E-mail address: mouheb.chebbi@irsn.fr (M. Chebbi).

https://doi.org/10.1016/j.cartre.2022.100164

part, characterization results of the investigated adsorbents by different techniques (N_2-porosimetry, Hg-porosimetry, XRD, SEM/EDX, XPS, CHONS elemental analysis) are presented. In the second part, the adsorption behavior towards CH_3I is discussed in terms of adsorption isotherms and kinetics. Two configurations have been selected by varying temperature and relative humidity. The objective was to better assess their behavior under both normal operating and severe conditions.

2. Experimental section

2.1. Presentation of the investigated adsorbents

Five commercially available AC prepared from coconut shells were selected. According to the impregnation type, the investigated materials were classified into three categories:

(i) AC impregnated by KI and TEDA.
(ii) AC only impregnated by TEDA.
(iii) Non impregnated AC (studied in order to investigate the impregnation effect on the adsorption behavior).

The protocol synthesis of these commercial materials was not communicated by the supplier. The main steps can be nevertheless schematized as the following [15]: (i) treatment of raw materials (coconut shell for the nuclear field), (ii) pyrolysis and activation (under CO_2 or steam [16]) and (iii) finally TEDA and KI impregnations, according to procedures similar to some available patents for iodine species removal in the nuclear context [17,18].

A specific designation was used in the present study in order to take into account the differences existing between all the tested adsorbents. It includes the impregnation nature, TEDA content, AC type as well as the grain size. Hence, the tested materials were denoted as *xTEDA,KI/AC$_y$-G or g* where x is the mass percentage in TEDA, KI is only mentioned for AC impregnated with potassium iodide, y is a suffix number related to the supplier, G is used for samples having a grain size ranging from 1 to 5 mm and g is used for a lower grain size (about 0.5 mm). The first category of materials (grain size ranging from 1 to 5 mm) belongs to activated carbons implemented within the ventilation circuits of nuclear facilities [19]. Lower grain size is associated with activated carbons found within the commercial cartridges dedicated to monitoring applications (environment, radioprotection) or to protect workers in potentially contaminated areas with gaseous radioiodine species.

2.2. Physico-chemical characterization studies

Prior to sorption tests, detailed characterizations of the investigated activated carbons were performed in order to establish relationships between their main characteristics and CH_3I retention properties. The chemical composition was assessed from elemental analysis as well as X-ray photoelectron sectroscopy (XPS). Textural properties were deduced from a combination between N_2 adsorption/desorption isotherms at 77 K and Hg porosimetry.

2.2.1. Chemical analysis

Before elemental analysis, the residual moisture was eliminated at 105 °C. The elemental composition (C, H, N, S and O content) was analyzed with a *Thermo Finnigan AE1112 Series Flash* (see details in S1, ESI). The average data presented in this paper were obtained from two up to three replicates. Further information related to the semi-quantitaive distribution of iodine, metallic elements (such as Fe, Cu, Ag...) were obtained from Energy Dispersive-X-Ray Fluoresence spectrometry (ED-XRF) analysis. The average data obtained for dry and finely crushed adsorbents were deduced from two replicates and reported in the supplementary (Table S2, ESI)

X-ray photoelectron sectroscopy (XPS) analysis were carried out with the aim to gain insights on elements chemical speciation over the studied AC. Details related to the data aquisition as well as the spectra deconvolution are reported in the supplementary (see details in S2, ESI).

2.2.2. Textural properties

Textural properties were determined from N_2 adsorption/desorption isotherms at 77 K (*Micrometrics ASAP 2020).* This technique was useful to probe both micropores (d pore $<$ 2 nm [20]) and mesopores (2 nm $<$ d pore $<$ 50 nm [20]). Prior to each adsorption/desorption sequence, samples were outgassed in vacuum (about 4 Pa) at 80 °C for 48 h to remove most of adsorbed impurities without desorbing TEDA or KI molecules. Then, the temperature was cooled down to 77 K and the N_2 adsorption phase was started by increasing progressively the relative pressures (P/P_0) from 1.27×10^{-6} to 0.9903. The desorption was studied afterwards for P/P_0 values ranging from 0.990 to 0.101. Specific surface areas (S_{BET}) were deduced from BET equation [21]. Microporous volumes (V_{micro}) as well as the micropore size distribution (d_{micro}) were obtained according the HK (Horwath-Kawazoe) model [22]. Mesoporous volume (V_{meso}) was calculated from the BJH (Barrett, Joyner, Halenda) model applied on the desorption branch [23]. Finally, the total pore volume (V_{pore}) was measured from N_2 adsorption isotherms at $P/P_0 = 0.99$.

Additional experiments were also performed using a Hg-porosimeter (*Micrometrics Autopore IV*) to probe pore diameter ranging from 8 nm to 600 µm. A part of the mesoporosity (8 nm to 50 nm) as well as the whole macroporosity (d pore $>$ 50 nm) were then evaluated from this technique. The effective density of the studied activated carbons was also determined from this technique. Before analysis, dried samples were outgassed at 2800 Pa. Then, the mercury volume penetrating the porous structure of the AC (*"the intrusion phase"*) was measured at different pressures ranging from 2800 Pa to 206.8×10^5 Pa. Finally, *"the extrusion phase"* was studied for pressures decreasing from 206.8×10^5 Pa to about 1.38×10^5 Pa.

The textural properties deduced from these two techniques are reported in the Table 2 (Section 3.1) using their average values deduced from two up to three repetitions.

2.3. CH_3I gas-phase batch sorption experiments

2.3.1. General description

Batch CH_3I sorption tests were carried out at different conditions using an original experimental setup (Fig. 1), which could be divided into three parts:

- The first part is dedicated to the generation of constant and reproducible CH_3I concentrations from certified CH_3I/N_2 bottle (*Air products*, 1000 or 2000 ppmv) and *Brooks* mass-flow controllers (using Air as diluting gas).
- The second part is called *"the reactor system"* (see Fig. 1), where a given CH_3I concentration is kept in contact with a fixed AC mass under various conditions (temperature (T) and relative humidity (R.H.)). One reactor or multiple reactors may be used in this part depending on the desired information (adsorption kinetics/adsorption isotherms).
- The final part is dedicated to the detection methodology. It consists in a *PerkinElmer Gas Chromatograph 580*, coupled with a *Pulsed Discharge Helium Ionization Detector (PD-HID, VICI)*. The analytical parameters were optimized in order to ensure both a significant signal/noise ratio and a sufficient temporal resolution to finely monitor the CH_3I kinetic decay (see Table S1).

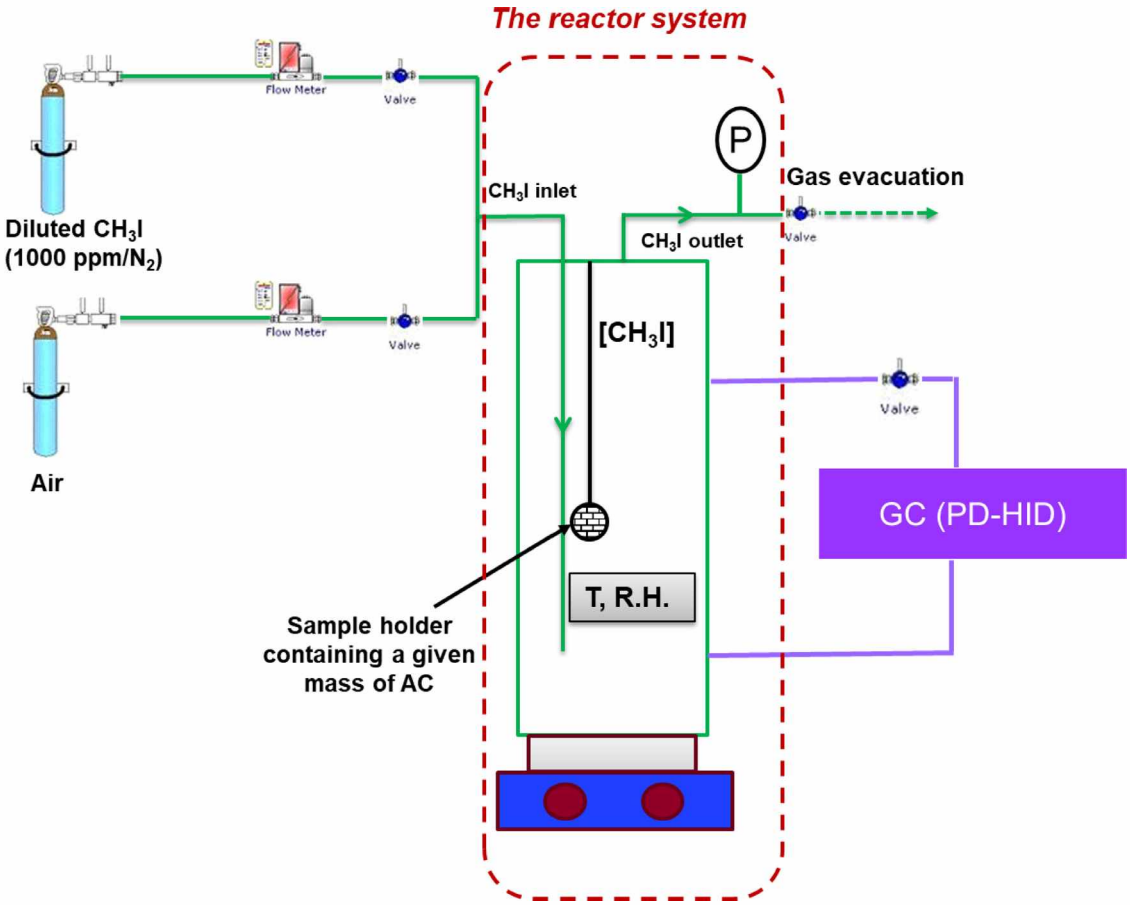

Fig. 1.. Experimental setup devoted to CH_3I adsorption by activated carbons under gas-phase batch conditions.

2.3.2. Experimental protocol

The experiments were achieved according to the following procedure:

The tested adsorbent previously dried at 105 °C was deposited into a stainless steel basket (mass between 50 mg and 100 mg), and introduced within the reactor middle (Fig. S1). A water recipient was placed on the reactor bottom in order to reach the desired relative humidity. A hygrometric probe (*HYGROSMART WR283-XP, Michell Instruments)* was implemented within the reactor in order to monitor Temperature (T) and Relative Humidity (R.H.) evolutions during an adsorption test (Fig. S2). In order to avoid the water vapor condensation, heating mats (*ACIM JOUANEN type*, 100 V, 40 W) were placed both on the walls and the upper part. Moreover, a K-type thermocouple was placed in the reactor middle, whose working temperature can be finely regulated (Fig. S1). The reactor bottom was also heated by a heating stirring plate for tests performed at 80 °C. The control of temperature homogeneity within the reactor was performed through different K-type measurement thermocouples placed at different points (Fig. S1). The online monitoring of (T, R.H.) data was performed by a homemade *LabVIEW* software to validate the operated conditions. Preliminary experiments were conducted with the aim to verify the possibility to achieve different operating conditions in terms of temperature and relative humidity (R.H.). Accordingly, some results are presented in the supplementary materials (Fig. S3). In conclusion, two conditions were tested in the present work:

- T = (35 ± 2)°C, R.H. = (26 ± 6) %, ([H_2O] ~ 15000 ppmv).
- T = (75 ± 2)°C, R.H. = (30 ± 5) %, ([H_2O] ~ 130000 ppmv).

The first configuration allowed exploring the AC performance under normal operating conditions within the nuclear facilities or power plants. This configuration was denoted afterwards as “normal operating conditions”. The second configuration was investigated in order to simulate degraded conditions, more comparable to an accidental situation within a nuclear reactor, as a comparison with the first conditions. This set of conditions was denoted in the following as “severe conditions”.

This experimental setup allowed us to investigate two complementary studies:

(i) Mono-reactor studies:

In this configuration, one reactor (free volume of 8 L) was used with the aim to establish the CH_3I adsorption kinetics (C_0 about 1000 ppmv) by various activated carbons (mass of 50–100 mg). Experiments were conducted under two specific conditions as stated previously. The online monitoring of CH_3I concentration in gaseous phase was performed until reaching the adsorption equilibrium.

Then, the cumulative adsorption capacity was determined according to a mass balance Eq. (1):

$$q_t = \frac{(C_0 - C_t) \times V}{m} \quad (1)$$

Where:

- q_t is the cumulative adsorption capacity (mol/g).
- C_0 is the initial CH_3I concentration (mol/L).
- C_t is the instantaneous CH_3I concentration (mol/L).
- V is the reactor volume (L).
- and m is the AC mass (g).

Table 1.
Chemical analysis of activated carbons as deduced from CHNSO elemental analysis.

Adsorbent	C (wt. %)	H (wt. %)	N (wt. %)	TEDA (wt. %)	O (wt. %)
AC_1-G	91.9 ± 1.5	0.456 ± 0.025	< D.L.	0	1.7 ± 0.4
1.6TEDA, KI/AC_1-G	87.15 ± 0.85	0.479 ± 0.048	0.400 ± 0.036	1.6	3.4 ± 1.2
2.4TEDA, KI/AC_2-g	85.6 ± 1.7	0.573 ± 0.034	0.600 ± 0.033	<=2.4	3.8 ± 1.4
2.0TEDA, KI/AC_3-G	84.9 ± 2.4	0.88 ± 0.16	0.500 ± 0.021	<=2.0	3.8 ± 1.2
3.0TEDA/AC_4-G	91.41 ± 0.41	0.754 ± 0.023	0.747 ± 0.019	<=3.0	3.5 ± 0.5

The temporal evolution of q_t was described according to an appropriate model in order to gain knowledge about CH_3I uptake rate and the duration required to achieve the adsorption equilibrium. This model will be detailed afterwards (Section 3.2.1, part a).

(i) Multi-reactor studies:

Seven identical reactors were used in order to establish CH_3I adsorption isotherms under the two investigated conditions. Different CH_3I concentrations ranging from 25 to 2000 ppmv have been contacted with a given adsorbent mass (50-100 mg) until the adsorption equilibrium at each inlet concentration. Then, adsorption capacity was deduced from the difference between initial and final CH_3I concentrations in gaseous phase. These reactors were handled simultaneously thanks to the use of an appropriate selector, which allowed quantifying the CH_3I concentration, depending on the selected reactor.

The obtained experimental adsorption isotherm was then described by a convenient model in order to have information about both the adsorption capacity at saturation and the energetic affinity displayed by a given adsorbent towards CH_3I.

3. Results and discussion

3.1. Characterization studies

3.1.1. Chemical composition

The chemical properties of the investigated AC as deduced from CHNSO elemental analysis are reported in the Table 1.

As expected, the investigated materials are essentially carbonaceous with carbon contents higher than 85 wt.% as deduced from elemental analysis. The XPS correspondent spectra are also characterized mainly by a strong carbon (C1s) line located at 285 eV (Fig. 2). The C1s spectra deconvolution has allowed determining the carbon speciation within the tested materials [24]. The obtained deconvolution spectra are predominated by graphitic sp^2 carbon (284.5 eV). The presence of other carbonated forms (acidic C=O bond, oxidized carbon in C-O-C bond…) can be also depicted to a lesser extent (Fig. S4 (A)). This carbon speciation is in agreement with the obtained broad XRD patterns for the studied AC (not shown here) typical of amorphous carbon structure [24,25].

The AC are also characterized by the presence of other elements in traces such as hydrogen and oxygen. These elements were reported to be assigned essentially from the physical activation process [16,26]. For comparison purposes, the H/C and O/C evolutions as a function of the tested AC is also presented in supplementary materials (Fig. S5). It can be seen that the 2.0TEDA,KI/AC_3-G could be distinguished by the highest hydrogen concentration with H/C ratio of 0.124 (Fig. S5). However, lower H/C ratios than 0.10 are recorded for the other AC. In addition, the increase of hydrogen concentration when moving from AC_1-G to 1.6TEDA,KI/AC_1-G may be attributed to an additional hydrogen supply from TEDA molecule ($C_6H_{12}N_2$). Very low values of O/C can be recorded especially for the non impregnated material (ratio of about 0.014, Fig. S5). The other adsorbents show the same oxygen concentrations with O/C values equal to approximately 0.03 (Fig. S5). Hence, the investigated materials seem to have a low hydrophilic character, in agreement with investigated application where a large content of water vapor is expected to be present [3,8].

Additional information about oxygen speciation can be deduced from the deconvolution of O1s XPS line located at 530 eV (Fig. S4 (B)) [27]. Accordingly, different oxygenated species can be distinguished such as conjugated C=O group (quinones, 530.8 eV), carbonyl C=O groups (532.1 eV), C-O-C group (ethers and alcohols, 533.2 eV), OH groups (C-OH in acid functional groups, 534.3 eV) and also condensed water (535.5 eV). From the comparison between the relative intensities of these peaks, it can be proposed that oxidized carbon is dominated mainly by ethers and carbonyls (Fig. S4 (B)).

TEDA incorporation within the tested materials can be evidenced firstly from elemental analysis. Indeed, nitrogen contents ranging from ((0.400 ± 0.036) wt.%, AC_1-G) to ((0.747 ± 0.019) wt.%, 3.0TEDA/AC_4-G) can be determined. An increasing evolution in N/C molar ratio can be also highlighted for the impregnated materials as the following (1.6TEDA/AC_1-G < 2.0TEDA,KI/AC_3-G < 2.4TEDA,KI/AC_2-g < 3.0TEDA/AC_4-G, Fig. S5). TEDA quantity can be deduced from nitrogen content by assuming that whole nitrogen functions are associated with TEDA. Such an approach may be used only for the 1.6TEDA,KI/AC_1-G material since the content of nitrogen can also be determined for the non-impregnated material (AC_1-G). Having no information about the native materials before impregnation for the other adsorbents, TEDA content can be considered as only an upper bound (Table 1). To sum-up, TEDA contents lower than 3 wt.% were obtained for the studied materials in agreement with the composition of *nuclear grade* activated carbons implemented in the ventilation circuits of nuclear facilities [8,28]. Additional insights about nitrogen speciation can be given from XPS characterizations (Fig. S4 (C)). For all the studied materials, the N1s line located at 400 eV was found to be composed by two contributions (N1 and N2 centered at 399 and 401 eV respectively, Fig. S4 (C)). By comparing the XPS spectra of AC_1-G and 1.6TEDA,KI/AC_1-G, a noteworthy increase due to N1 contribution was observed after TEDA introduction. However, a quasi-similar contribution from N2 was observed in both cases (Fig. S4 (C)). Consequently, the N1 component may be assigned to TEDA molecule. Furthermore, this contribution was related to N-Csp^3 bonds, as expected in intact TEDA molecule [29]. However, the N2 contribution may be associated with N-Csp^2 bonds. A similar behavior can be noticed for 2.4TEDA,KI/AC_2-g and 3.0TEDA/AC_4-G materials, where the N1s line was characterized by a dominant N1 component due to TEDA and a residual N2 contribution coming probably from the native materials (Fig. S4 (C)). Hence, it is worthy to recall that TEDA contents deduced from CHNSO analysis should be expressed using an upper bound as stated before. Furthermore, the presence of N-Csp^3 bonds type indicates that the introduced TEDA did not react neither with the carbon surface nor with KI. Therefore, the possible $\{TEDA^+I^-\}$ salt formation as reported previously by Hayashi [29] was not observed during the present work. Consequently, the nitrogen speciation seems to be rather the same between the TEDA impregnated sorbents (without KI) and the TEDA/KI co-impregnated AC.

KI impregnation has been experimentally evidenced from both XPS and ED-XRF spectrometric (Fig. S4 (D) and Table S2) analy-

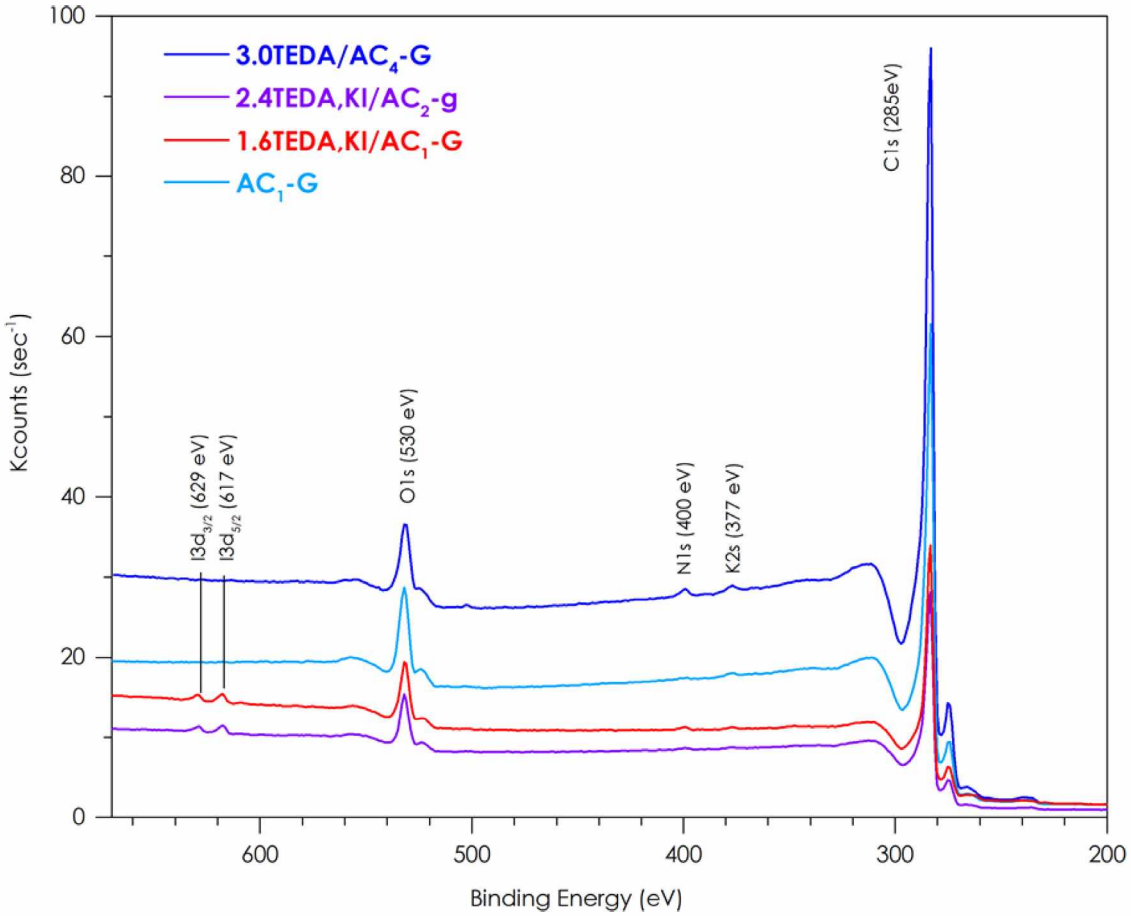

Fig. 2.. XPS spectra for some activated carbons.

sis for 1.6KI,TEDA/AC_1-G, 2.0TEDA,KI/AC_3-G and 2.4TEDA,KI/AC_2-g adsorbents. More particularly, the I3d XPS line was found to be composed by two distinct contributions (Fig. S4 (D)): (i) the first one at 618 eV is associated to I^- characteristic of KI according to the NIST XPS database [30]; (ii) the second line is rather associated to a less negative iodide [30]. The potassium was observed for all the studied adsorbents, even for the non impregnated AC (Fig. S4 (E) and Table S2). From ED-XRF spectrometric analysis (Table S2), the calcium has been only observed for adsorbents without KI. By comparing AC_1-G and 1.6TEDA,KI/AC_1-G (Table S2), it can be proposed that KI impregnation occurs on the detriment of calcium sites. In addition, metal oxides traces containing mainly copper and iron can also be detected for the tested materials. It has been reported that these elements may act as secondary adsorption sites towards CH_3I [31].

Finally, the presence of silver sites by ED-XRF analysis (Table S2) was only observed for the 3.0TEDA/AC_4-G, as a comparison with the other adsorbents. The presence of this element was also proved by other characterizations techniques such as SEM-EDX and XRD analysis (Fig. S6).

3.1.2. Textural properties

(a) *N_2 adsorption/desorption tests at 77K*

The obtained N_2 adsorption isotherms according to the procedure detailed in the experimental part (Section 2.2.2) are presented in supplementary (Fig. S7). It can be revealed that all the recorded graphs exhibit a type I isotherm, typical of microporous materials [32]. The small hysteresis presence can be also noticed, indicating the presence of some mesopores with narrow openings [33]. The associated textural properties are reported in the Table 2, as average values of two up to three replicates.

Generally, high specific surface areas (Table 2) can be highlighted for the tested adsorbents, with values ranging from (1014 ± 50) m^2/g (2.0TEDA,KI/AC_3-G) to (1213 ± 62) m^2/g (3.0TEDA/AC_4-G). In addition, the studied AC display a significant microporous character (V_{micro}/V_{pore} > 0.89, Table 2), in agreement with the use of coconut shell as raw material. Indeed, this raw material is known to be associated with the fabrication of highly microporous AC [16,34,35]. Moreover, a mean micropore diameter ranging from 0.55 nm (2.0TEDA,KI/AC_3-G) to 0.59 nm (2.4TEDA,KI/AC_2-g) can be deduced according to the HK formalism (Table 2). This property is known to be suitable for CH_3I capture (kinetic diameter of 0.5-0.6 nm [7]) by physisorption phenomena. A less pronounced contribution due to mesopores is observed generally for the tested materials except the 2.0TEDA/KIAC_3-G adsorbent, characterized by a relatively higher mesoporous character (Fig. S7 and Table 2).

Let's now discuss about the impregnation effect on textural properties of the investigated AC. The comparison between AC_1-G and 1.6TEDA,KI/AC_1-G reveals a decrease of about 8 % in S_{BET} and V_{micro} parameters after impregnation. The impregnation effect cannot be however elucidated with accuracy for the other impregnated AC due to the lack of information on the starting materials (*i.e.* before KI and TEDA impregnation). Nevertheless, pore blockage phenomena are known to occur upon impregnation due to the presence of the incorporated agents within or at the micropores openings [9,12,16,36,37].

Considering the Hg porosimetry results of the studied AC, relevant information to macroporous volumes and the effective densi-

Table 2.
Textural properties of the investigated adsorbents from both N_2 and Hg porosimetries.

Adsorbent	N_2 adsorption/desorption tests (77 K)					Mercury porosimetry	
	S_{BET} (m^2/g)	V_{micro} (cm^3/g)	d_{micro} (nm)	V_{meso} (cm^3/g)	V_{pore} (cm^3/g)	V_{macro} (cm^3/g)	$\rho_{effective}$ (g/cm^3)
AC_1-G	1128 ± 20	0.470 ± 0.001	0.564 ± 0.001	0.056 ± 0.001	0.510 ± 0.004	0.103 ± 0.002	0.550 ± 0.006
1.6TEDA, KI/AC_1-G	1028 ± 50	0.431 ± 0.005	0.555 ± 0.005	0.027 ± 0.005	0.451 ± 0.005	0.140 ± 0.004	0.591 ± 0.005
2.4TEDA, KI/AC_2-g	1145 ± 50	0.471 ± 0.013	0.59 ± 0.01	0.066 ± 0.002	0.52 ± 0.02	N.D.	N.D.
2.0TEDA, KI/AC_3-G	1014 ± 50	0.423 ± 0.002	0.550 ± 0.002	0.072 ± 0.005	0.475 ± 0.008	0.24 ± 0.01	0.486 ± 0.001
3.0TEDA/AC_4-G	1213 ± 62	0.503 ± 0.026	0.579 ± 0.004	0.070 ± 0.004	0.554 ± 0.029	N.D.	N.D.

ties have been deduced (Table 2). On the one hand, V_{macro} ranging from (0.103 ± 0.002, AC_1-G) cm^3/g to (0.24 ± 0.01, 2.0TEDA,KI/AC_3-G) can be recorded for the considered adsorbents. These results seem to be in line with previous works. Indeed, it has been reported that activated carbons derived from coconut shell are generally characterized by a bimodal distribution in pore size, with a dominant microporous character, and a less pronounced contribution due to macroporosity [16,35]. On the other hand, the calculated effective densities (Table 2) are consistent with reported values for AC implemented in the nuclear field [38]. Indeed, AC having grain size distribution between 1 and 5 mm are characterized by $\rho_{effective}$ values ranging from (0.486 ± 0.001) g/cm^3 to (0.591 ± 0.005) g/cm^3.

3.2. Screening study at batch reactor system under variable operating conditions (T, R.H.)

3.2.1. CH_3I adsorption kinetics

(a) Theoretical aspects about kinetics modeling

Several diffusion mechanisms may be involved during CH_3I adsorption by the studied activated carbons. Generally, the mass transfer global resistance can be supposed as the resultant from two main contributions [39–41]: (i) external mass transfer and (ii) intra-particular mass transfer. In the case of porous adsorbents such as activated carbons, it is known that the adsorption rate in the porous framework is rather controlled by the step (ii) than the step (i) [39]. Moreover, experimental precautions (moderate stirring) were undertaken in order to neglect the phenomena due to the external mass transfer, as stated in the previous part (Section 2.3). The flow within an ideal particle (of spherical geometry) can be in turn divided in two main categories [39,41]: the first one is related to the gas phase diffusion within the pore according to molecular and Knudsen mechanisms. The second contribution is attributed to the surface diffusion in the adsorbed phase.

In the present study, the linear driving force model (LDF) [42] was proposed in order to simulate the CH_3I uptake curves:

$$\frac{\partial q\,(t)}{\partial t} = K_g \times (q^* - q\,(t)) \tag{2}$$

Where:

- q: the average concentration within the adsorbed phase (mol/g)
- q^*: the equilibrium concentration (mol/g)
- K_g: the global mass transfer coefficient (s^{-1}).

In this model, the difference between the bulk phase and the adsorbed phase concentrations represents the driving force of adsorption. This model displays numerous advantages. It has a simple mathematical solution that has been widely used in order to describe the uptake kinetics for multiple systems [39,43]. In addition, all these mass transfer resistances are lumped together in one single barrier represented by the global mass transfer coefficient (K_g) [39,44].

In order to test the application of the LDF model to our experimental data, a method of least square was applied to search for the minimum in residuals between experimental and theoretical data. The global mass transfer coefficient can be then deduced from the linear regression:

$$\theta = \frac{q}{q^*} = 1 - \exp(-K_g t) \tag{3}$$

The determination of this constant may give valuable information about the facility of CH_3I molecules transport. In other words, it was notified that ($1/K_g$) could be seen as a characteristic time constant for the adsorption kinetics [41]. More particularly, it is possible to gain knowledge about the diffusion rate limiting steps depending on the investigated conditions, by a combination between the calculated transport coefficients and the physicochemical properties of the studied AC.

b) Results

The obtained kinetic curves for CH_3I adsorption on the investigated sorbents as well as their LDF fittings are presented in the supplementary (Fig. S8, ESI). The main results of LDF modeling for the two studied conditions are reported in the Table 3.

Generally, the obtained experimental curves in the two studied conditions displayed a rather similar shape. Indeed, a progressive increase in the adsorbed amount is observed during the first adsorption stages, accompanied then by a plateau indicating the surface saturation. This plateau corresponds to the adsorption capacity at the equilibrium (q^*) for given experimental conditions (C_0, $m_{adsorbent}$, T and R.H.). Our attempts to model the filling of free adsorption sites according to the LDF model are found to be satisfying, especially in the first set of conditions ($R^2 > 0.9873$, Table 3). The deduced adsorption capacities at the equilibrium are higher than 100 mg/g at T = (35 ± 2)°C, R.H. = (26 ± 6) % ([H_2O] ~ 15000 ppmv). The computed adsorption capacities in these conditions seem to be in good agreement with the values reported in the literature for various activated carbons when initial CH_3I concentrations ~~of~~ are about 1000 ppmv [45].

In the second set of conditions (T = 75°C, [H_2O] ~ 130000 ppmv), lower correlation coefficients were in contrast obtained ($R^2 < 0.9885$, Table 3). This behavior may be explained by a more significant amount of water vapor, whose condensation may be sometimes difficult to be avoided. The more pronounced occurrence of chemical reactions in those conditions may be also invoked. This was the case for the 3.0TEDA/AC_4-G adsorbent (R^2 = 0.9413, Table 3). An empiric *dual LDF* model [46,47] was therefore proposed in order to describe the CH_3I adsorption kinetic by this adsorbent:

$$\theta = A \times (1 - \exp(-K_1 t)) + (1 - A) \times (1 - \exp(-K_2 t)) \tag{4}$$

This model assumes the presence of two barriers in the diffusion process, represented by two mass transfer constants (K_1 and K_2) respectively and an empirical A constant correspondent to the relative contribution of each barrier [46]. The compilation of this model provided a better fit to the experimental data obtained for 3.0TEDA/AC_4-G (R^2 =0.9690). In that respect, two adsorption sites can be distinguished: (i) the first component was characterized by a slow diffusion process (K_1 = 0.0089 ± 0.0011 s^{-1}), but with a higher occurrence probability (A = 0.768 ± 0.087), (ii) the second one corresponds to a faster process (K_2 = 0.066 ± 0.038 s^{-1}), with a lower contribution (1-A = 0.23).

Table 3.
Summary of kinetic results from the linear driving force model in the two selected conditions.

Adsorbent	C_0 = (774 ± 20) ppmv T = (35 ± 2)°C, R.H. = (26 ± 6) % [H_2O] ~ 15000 ppmv			C_0= (852 ± 34) ppmv T = (75 ± 2)°C, R.H. = (30 ± 5) % [H_2O] ~ 130000 ppmv		
	q^* (g/g)	K_g LDF (s^{-1})	R^2	q^* (g/g)	K_g LDF (s^{-1})	R^2
AC_1-G	0.1501 ± 0.0022	0.02280 ± 0.00025	0.9953	0.0284 ± 0.0011	0.0208 ± 0.0011	0.9677
1.6TEDA, KI/AC_1-G	0.1379 ± 0.0019	0.02494 ± 0.00028	0.9956	0.03514 ± 0.00064	0.01901 ± 0.00051	0.9885
2.4TEDA, KI/AC_2-g	0.1245 ± 0.0023	0.03457 ± 0.00039	0.9945	0.0316 ± 0.0014	0.01593 ± 0.00088	0.9616
2.0TEDA, KI/AC_3-G	0.1438 ± 0.0022	0.02831 ± 0.00045	0.9873	0.03463 ± 0.00061	0.01813 ± 0,00082	0.9713
3.0TEDA/AC_4-G	0.1518 ± 0.0051	0.01692 ± 0.00021	0.9906	0.0541 ± 0.0011	0.01219 ± 0.0005	0.9421

In addition, equilibrium adsorption capacities (q^*) ranging from 30 to 50 mg/g were computed in this set of conditions (Table 3). This adsorption capacity drastic decrease as a comparison with "normal operating conditions" is explained by both the temperature increase and the more pronounced presence of water vapor, according to previous works [8,48,49]. This deterioration in retention performance will be further investigated in terms of adsorption capacities at saturation as deduced from adsorption isotherms (Section 3.2.2).

Let us now focus on the determination of the kinetic limiting step for CH_3I removal by the studied materials depending on the studied condition. For a comparison purpose, only the LDF model was considered with the aim to assess the most prominent factors towards CH_3I mass transfer inside the tested adsorbents. The comparison of the obtained diffusion constants with some adsorbents properties is depicted in the Fig. 3. Different trends can be noticed depending on the experimental conditions. In the first set of conditions, CH_3I adsorption is mainly governed by physisorption phenomena [8,9,12,49]. These phenomena are known to be almost sensitive to the micropore accessibility especially in the case of CH_3I (kinetic diameter of 0.5-0.6 nm) [8,50]. Hence, the uptake rate of CH_3I will be mainly determined by the textural properties as deduced from N_2 adsorption isotherms at 77 K. In other words, an increase of adsorption sites number will be expected for higher specific surface areas (S_{BET}) considering the first set of conditions [43]. Therefore, the associated kinetic time required to fill all the free adsorption sites will be higher. Consequently, a decrease of the mass transfer constant (K_g) will occur. In that respect, a quasi-linear decreasing relationship is obtained between the global mass transfer coefficient (K_g) and the BET specific surface area for adsorbents displaying a rather similar grain size distribution (Fig. 3 (A)). In contrast, a significant deviation from the linear fit in Fig. 3 (A) is observed in the case of the 2.4TEDA,KI/AC_2-g, displaying the highest adsorption rate (K_g= 0.03457 ± 0.00039 s^{-1}, Table 3). This behavior can be assigned to its relatively low grain size (about 0.5 mm) as a comparison with the other adsorbents (grain size ranging from 1 to 5 mm). Indeed, lower diffusional constraints are expected for decreasing grain size [43].

In the second set of conditions, the main process involved in CH_3I uptake is the chemical reaction occurring between the TEDA active sites and CH_3I [8,9,12,42]. In that respect, a linear decreasing relationship was established for impregnated adsorbents between K_g and the N/C ratio, as measured from elemental analysis (Fig. 3 (B)).

In the next section, a peculiar attention will be devoted to the adsorption isotherms. More particularly, retention performance towards CH_3I in the two selected conditions will be discussed in terms of the adsorption capacity at saturation as well as the interaction strength.

3.2.2. CH_3I adsorption isotherms

(a) Adsorption isotherms modeling

In the present study, the experimental data were mainly fitted using the Langmuir model [51] represented by the following equation:

$$q = \frac{q_m \times b \times C_e}{1 + b \times C_e} \tag{5}$$

Where:

- q (g/g): the adsorption capacity determined experimentally for each concentration;
- q_m (g/g): the maximal adsorption capacity corresponding to the saturation of the active sites towards CH_3I;
- b (m^3/mol): the Langmuir affinity coefficient;
- C_e (mol/m^3): the CH_3I concentration at the adsorption equilibrium.

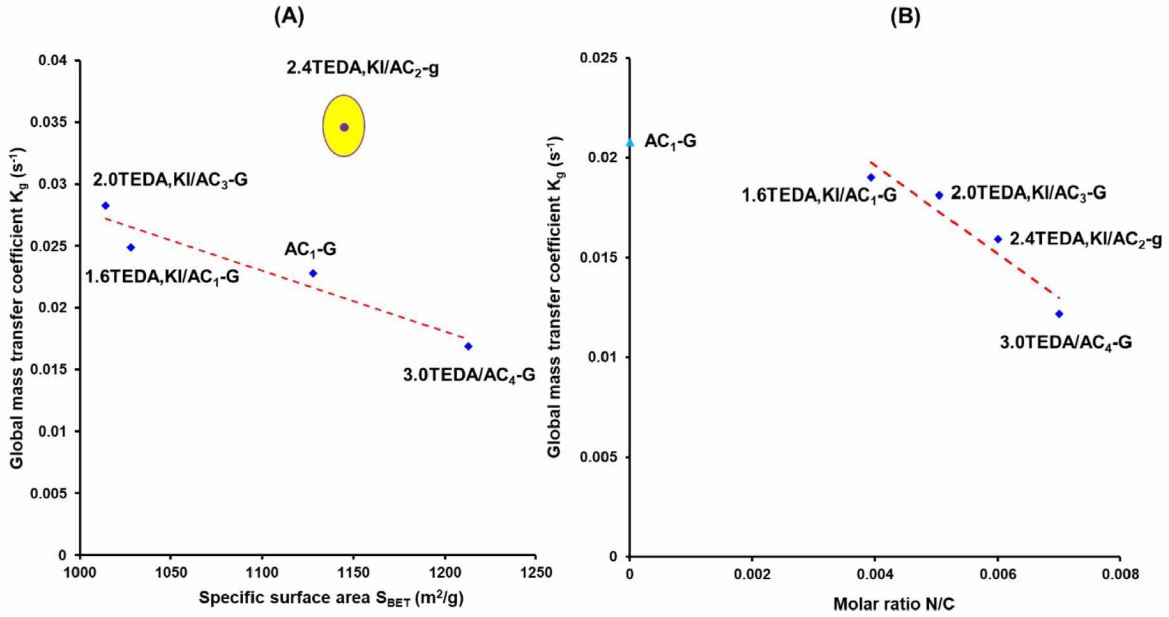

Fig. 3.. Determination of the influencing parameters towards the mass transfer constant (K_g) for the two investigated configurations: (A) « normal operating conditions" and (B) « severe conditions ».

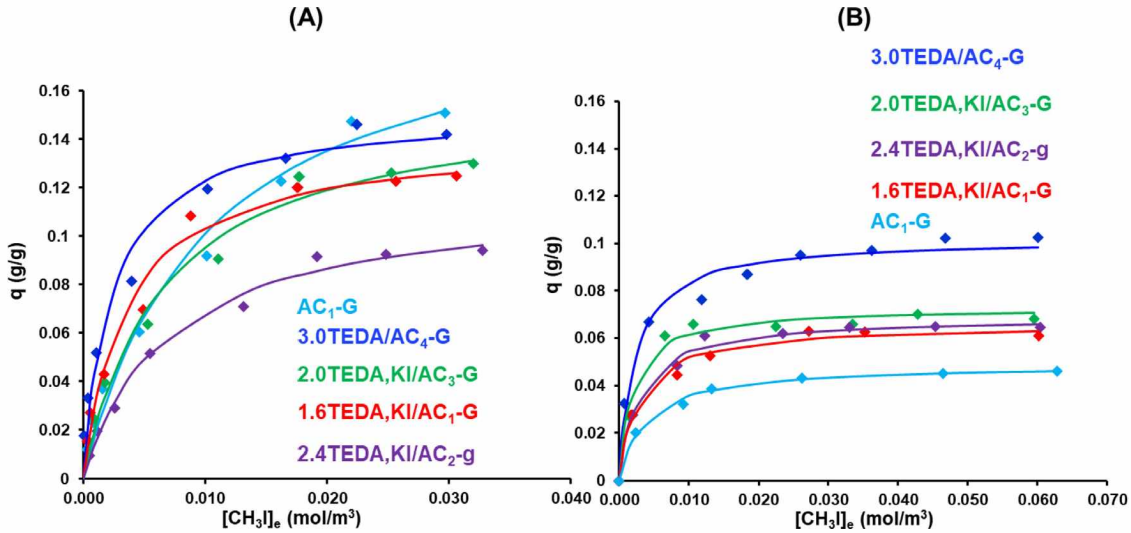

Fig. 4.. Experimental CH_3I adsorption isotherms and Langmuir fitted models obtained with the studied activated carbons for the two investigated configurations: (A) normal operating conditions; (B) severe conditions.

This model was found to be a useful formalism to describe both physical and chemical adsorption [52]. In this formalism, the adsorbent surface is considered to be energetically homogeneous. Adsorption sites are characterized by a global affinity coefficient (*b*), related to the interaction strength [52]. Hence, the determination of this coefficient may give valuable information about the trapping stability.

In some cases, the Dubinin-Astakhov (DA) model [53] was used to take into account the heterogeneous character of adsorbents surface. Indeed, the DA equation allowed us to plot the CH_3I adsorption energy distribution [52], from data obtained in "normal operating conditions".

(b) Results

CH_3I Adsorption isotherms were determined in the selected conditions (T, R.H.) through the multi-reactor configuration of the batch reactor system, as stated previously (Section 2.3). The experimental curves were described according to the Langmuir model. The fitting results are shown in Fig. 4 and the corresponding modeling parameters are listed in Table 4.

Different trends were found depending on temperature and relative humidity (Fig. 4). First, relatively good adsorption performance can be outlined for all the tested adsorbents at "normal operating conditions" (Table 4 and Fig. 4 (A)). Indeed, the maximal adsorption capacities (as deduced from Langmuir model) are ranging from (0.1171 ± 0.0053) to (0.204 ± 0.017) g/g for 2.4TEDA,KI/AC_2-g and AC_1-G respectively (Table 4). Taking into account only the computed adsorption capacities values, the non impregnated activated carbon (AC_1-G) seems to display the best adsorption performance towards CH_3I in the first set of conditions. This behavior is in line with literature studies [36,48,49] considering similar conditions in terms of temperature, relative humidity and concentrations. Indeed, it has been reported that adsorption is mainly governed by physisorption at low temperatures, dry atmosphere and at high adsorbate concentrations [9,36,48,49]. In

Table 4.
Results of CH_3I adsorption isotherms fitting with the langmuir model in both « normal operating" and "severe" conditions.

Adsorbent	T = (35 ± 2)°C, R.H. = (26 ± 6) % [H_2O] ~ 15000 ppmv			T = (75 ± 2)°C, R.H. = (30 ± 5) % [H_2O] ~ 130000 ppmv		
	q_m (g/g)	b (m^3/mol)	R^2	q_m (g/g)	b (m^3/mol)	R^2
AC_1-G	0.204 ± 0.017	98 ± 21	0.986	0.0487 ± 0.0011	259 ± 27	0.996
1.6TEDA, KI/AC_1-G	0.1414 ± 0.0068	276 ± 52	0.983	0.0658 ± 0.0024	341 ± 69	0.985
2.4TEDA, KI/AC_2-g	0.1171 ± 0.0053	142 ± 20	0.992	0.0695 ± 0.0017	348 ± 50	0.991
2.0TEDA, KI/AC_3-G	0.1581 ± 0.0097	152 ± 30	0.984	0.0725 ± 0.0023	516 ± 106	0.982
3.0TEDA/AC_4-G	0.1523 ± 0.0086	422 ± 113	0.971	0.1022 ± 0.0031	446 ± 89	0.981

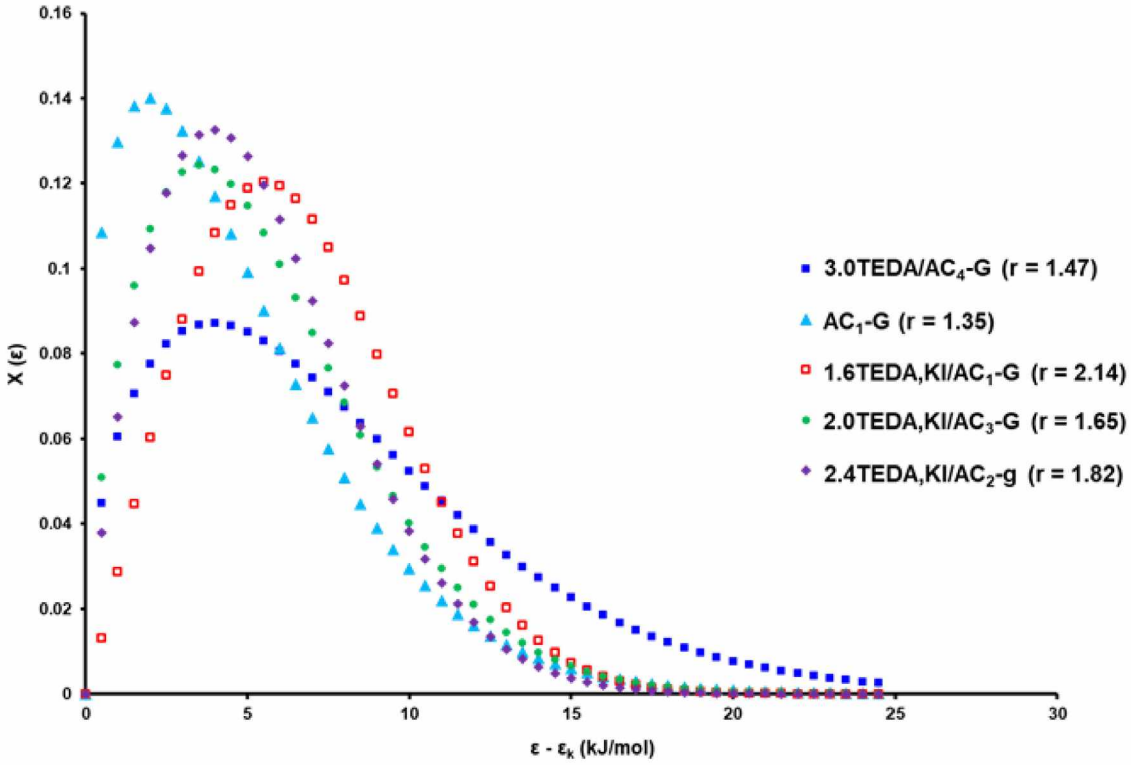

Fig. 5.. CH_3I Adsorption energy distribution curves deduced from the DA model for the studied adsorbents (T = (35 ± 2)°C, R.H. = (26 ± 6) %, [H_2O] ~ 15000 ppmv).

addition, these phenomena are known to be more sensitive to the microporous network accessibility than to the chemical properties of the sorbent. As stated in the characterization section, TEDA and KI impregnations induces a partial blockage of the adsorbents microporosity, leading therefore to a detrimental effect towards CH_3I capture. This fact can be elucidated more particularly when comparing the obtained performance for AC_1-G and 1.6TEDA,KI/AC_1-G materials. Indeed, the computed q_m (Table 4) values are decreasing from (0.204 ± 0.017) to (0.141 ± 0.007) g/g when moving from AC_1-G to 1.6TEDA,KI/AC_1-G respectively.

Nevertheless, TEDA functionalization enhances the chemical reactions leading to a specific storage of CH_3I molecules as stated in previous works [9–12]. Then, an increase of the energetic affinity displayed by the activated carbon towards CH_3I is expected. These considerations are in line with the significant increase of the Langmuir coefficient from (98 ± 21) to (276 ± 52) m^3/mol after TEDA incorporation within the AC_1 activated carbon (Table 4). Among all the investigated materials, the 3.0TEDA/AC_4-G adsorbent exhibits the highest energetic affinity (according to the Langmuir model) towards CH_3I (Table 4). The obtained adsorption energy distribution as deduced from the Dubinin-Astakhov formalism (Fig. 5) gives also similar conclusions. Indeed, a progressive broadening of the curves can be depicted after the progressive TEDA incorporation as a comparison with the non impregnated adsorbent, due to the simultaneous occurrence of physical and chemical interactions for CH_3I capture [52].

The most pronounced widening can be evidenced especially for the 3.0TEDA/AC_4-G sorbent (with adsorption sites at 20-25 kJ/mol, Fig. 5). The superior affinity observed for this sorbent can be explained by its relatively higher TEDA content (Table 1) as concluded from elemental analysis. The presence of silver traces as shown by SEM-EDX and XRD techniques (Fig. S6) may also be proposed, owing to their high reactivity with iodine species [31,54,55].

When considering the second set of conditions (Fig. 4 (B) and Table 4), a decrease of adsorption performance can be outlined for all the tested adsorbents. Indeed, the computed adsorption capacities as deduced from Langmuir model are ranging from (0.0487 ± 0.0011) to (0.1022 ± 0.0031) mg/g (Table 4). This deterioration in retention properties is assigned to an increase in both the adsorption temperature (from 35 to 75 °C) and the water vapor content (from 15000 to about 130000 ppmv). On the one hand, the presence of water vapor in large excess is known to induce an adverse effect on CH_3I trapping by activated carbons, due to the adsorption competition between CH_3I and H_2O molecules [8,9,48]. More precisely, it was reported [56] that the adsorbed water molecules formed clusters interacting through hydrogen bonds with activated carbon porous network, making therefore the active sites less accessible for iodine species. On the other hand, the

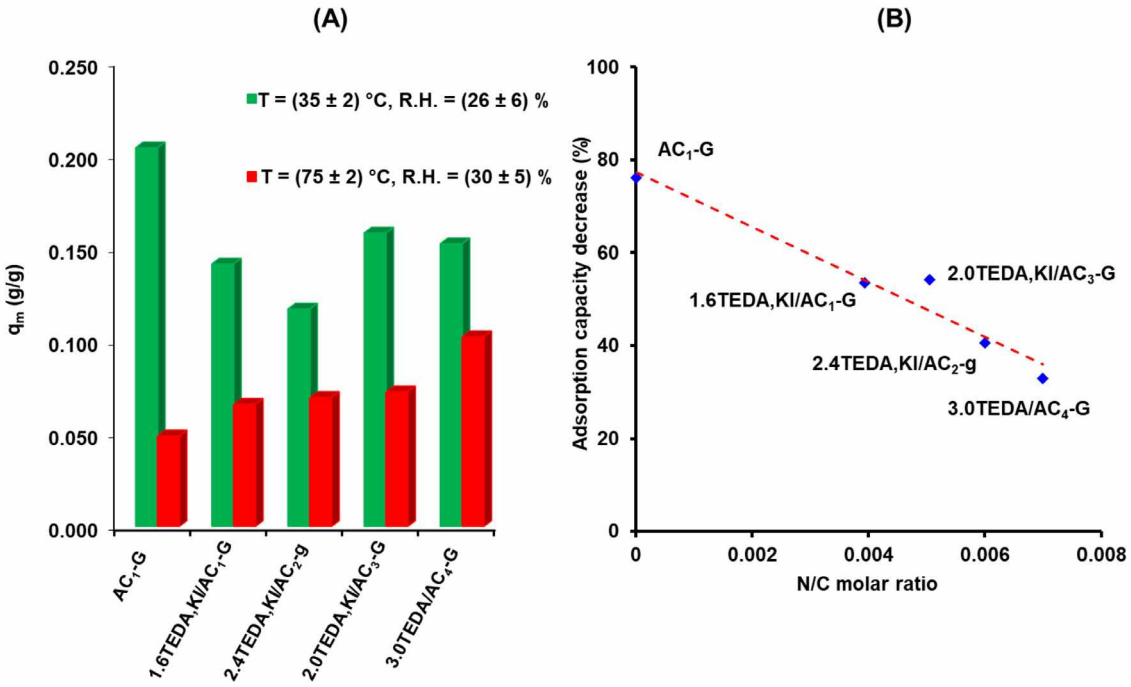

Fig. 6.. (A) influence of experimental conditions on the adsorption capacities deduced from Langmuir model, (B) evolution of the adsorption capacity decrease as a function of the N/C molar ratio.

global adsorption capacities decrease is reported by several studies for increasing temperature owing to the reduction of physisorption phenomena, which are promoted preferentially at low temperatures [36,49]. More particularly, the study of Park et al. [49] have reported a progressive decrease in the fraction of physisorbed CH_3I by an impregnated AC (6.5 wt% of TEDA) from 58% to 34% for temperatures ranging from 35 to 75 °C.

During the present study, the decrease extent in adsorption capacities is dependent on the activated carbon nature (Fig. 6 (A)). As expected, the most detrimental effect was observed for the non impregnated adsorbent, where only no specific interactions are known to be involved for CH_3I capture [8]. More precisely, about 76% of decrease in adsorption capacities is outlined when moving from the first to the second set of conditions for the AC_1-G material (Table 4, Fig. 6). In that respect, TEDA impregnation is essential in order to overcome the effects related to water vapor and temperature in agreement with numerous studies [9–12]. Recently, TEDA impregnation has been proved by DFT calculations to improve the retention performance of activated carbons by freeing the active sites of the support, thanks to the strong affinity displayed by water for TEDA molecules [12]. In addition, it is known that the fraction of chemisorbed CH_3I is increased for higher temperatures as a comparison with other mechanisms (especially physisorption) [49]. Then, the chemical reactivity of TEDA with CH_3I will be enhanced at higher temperatures. The obtained results (Table 4 and Fig. 6) indicate a progressive improvement in retention performance at "severe conditions" for increasing nitrogen content. Hence, a decrease of only 33% in the adsorption capacity is obtained for the 3.0TEDA/AC_4-G sorbent characterized by the highest content in TEDA. More precisely, a quasi-linear relationship can be deduced between the q_m decrease magnitude and the N/C molar ratio for all the considered adsorbents (Fig. 6 (B)). According to this relationship, TEDA impregnation seems to be required in order to ensure a stronger fixation of CH_3I at more stringent conditions in agreement with the previous findings [8,9,12]. Nevertheless, a closer look to the obtained evolution (Fig. 6 (B)) indicates a small deviation in the case of the 2.0TEDA,KI/AC_3-G material. The most pronounced mesoporous character for this adsorbent as stated in the characterization section (Table 2 and Fig. S7) may be responsible for that behavior. Indeed, the presence of mesopores is known to promote the adsorption of water molecules, namely according to capillary condensation mechanism [57].

Among the investigated adsorbents, the 3.0TEDA/AC_4-G adsorbent seems to display the best sorption performance towards CH_3I under the studied conditions in terms of temperature and relative humidity. This adsorbent exhibits a well-developed microporous network constituting a key factor for the trapping of CH_3I under "normal operating conditions". In addition, its superior ability to retain CH_3I under "severe conditions" may arise essentially from its highest content of TEDA, but also from the presence of some silver species as proved by XRD and SEM/EDX characterizations.

4. Conclusions

This study aimed to unravel the relationships existing between the physico-chemical properties of some activated carbons and their ability to trap CH_3I as a function of the experimental conditions. More precisely, the effect of impregnation was considered on the sorption performance displayed by activated carbons towards CH_3I.

Results were dependent on the investigated configuration. More particularly, it has been shown that CH_3I adsorption properties are mainly sensitive to the microporous network availability in configurations mainly governed by physical adsorption (low temperature, high adsorbate concentration and low water vapor content). In that respect, the progressive impregnation with KI and TEDA induces a decrease of the global adsorption capacity as a correlation with porosity partial blocking phenomena, due to the presence of these molecules within the internal porosity. In contrast, the TEDA presence seems to be crucial in order to ensure a stronger and more specific storage of CH_3I molecules through chemical reactions. This contribution is primordial in order to guarantee an accepted retention behavior towards CH_3I at higher temperature and in the presence of water vapor in large excess. In addition, the present study

has shown a quasi-linear relationship between the adsorption capacity and the TEDA content under the investigated conditions ($T = (75 \pm 2)°C$, R.H. $= (30 \pm 5)$ %, $[H_2O] \sim 130000$ ppmv). Our attempts to model the sorption kinetics through the LDF model have also noticed similar conclusions, highlighting that adsorption uptake is mainly governed by the amount of TEDA molecules.

These works represent a promising milestone to assess the more influencing parameters towards the removal of CH_3I by activated carbons under batch reactor configuration (kinetics and adsorption isotherms). Additional investigations will be conducted at semi-pilot scale within the PERSEE facility of IRSN. The main objectives will be to elucidate the importance of adsorbents properties towards CH_3-^{131}I decontamination factors (DF). Moreover, a peculiar attention will be devoted to better assess the contribution as well as the mechanism of isotopic exchange reaction involved during the capture of CH_3-^{131}I by $K^{127}I$-impregnated activated carbons.

Declaration of Competing Interest

The authors declare that they have no known competing financial interests or personal relationships that could have appeared to influence the work reported in this paper.

Acknowledgments

This work has been supported by the French State under the program "Investissements d'Avenir MiRE managed by the ANR under grant agreement ANR-11-RSNR-0013-01.

Supplementary materials

Supplementary material associated with this article can be found, in the online version, at doi:10.1016/j.cartre.2022.100164.

References

[1] B. Clement, L. Cantrel, G. Ducros, F. Funke, L. Herranz, A. Rydl, G. Weber, C. Wren, State of the art report on iodine chemistry, in: OCDE Report, Nuclear Energy Agency Committee on the Safety of Nuclear Installationsnea/CSNI/R, 2007, p. 1.
[2] D.R. Haefner, T.J. Tranter, Methods of Gas Phase Capture of Iodine from Fuel Reprocessing Off-Gas: A Literature Survey, Idaho National Laboratory, 2007 INL/EXT-07e12299.
[3] L. E. Herranz, T. Lind, K. Dieschbourg, E. Riera, S. Morandi, P. Rantanen, M. Chebbi, N. Losch, PASSAM "State-of-the-art report, Technical Bases for Experimentation on Source Term Mitigation Systems", PASSAM THEOR-T04 [D2.1], Passam Project, 2013.
[4] R.E. Adams, Removal of iodine from gas streams, in: Proceedings of the 7th EAC Air Cleaning Conference, Brookhaven National Laboratory, New York (USA), 1961 October 10/12.
[5] R.T. Jubin, Airborne Waste Management Technology Applicable for Use in Reprocessing and Plants for Control of Iodine and Other Off-Gas Constituents, Oak Ridge National Laboratory, 1988 Report ORNL/TM-10477.
[6] R.T. Jubin, A Literature Survey of Methods to Remove Iodine from Off-Gas Streams Using Solid Sorbents, Oak Ridge National Laboratory, 1979 Report ORNL-TM-6607.
[7] R.D. Scheele, L.L. Burger, C.L. Matsuzaki, Methyl Iodide Sorption by Reduced Silver Mordenite, Pacific Northwest Laboratory, 1983 PNL-4489.
[8] J. Huve, A. Ryzhikov, H. Nouali, V. Lalia, G. Augé, T.J. Daou, Porous sorbents for the capture of radioactive iodine compounds: a review, RSC Adv. 8 (2018) 29248–29273.
[9] K. Ho, S. Moon, H.C. Lee, Y.K. Hwang, C.H. Lee, Adsorptive removal of gaseous methyl iodide by triethylenediamine (TEDA)- metal impregnated activated carbons under humid conditions, J. Hazard. Mater. 368 (2019) 550–559.
[10] E. Aneheim, D. Bernin, M.R.S.J. Foreman, Affinity of charcoals for different forms of radioactive organic iodine, Nucl. Eng. Des. 328 (2018) 228–240.
[11] H. Chun, J. Kang, B. Han, First principles computational study on the adsorption mechanism of organic methyl iodide gas on triethylenediamine impregnated activated carbon, Phys. Chem. Chem. Phys. 18 (2016) 32050–32056.
[12] K. Ho, H. Chun, H.C. Lee, Y. Lee, S. Lee, H. Jung, B. Han, C.H. Lee, Design of highly efficient adsorbents for removal of gaseous methyl iodide using tertiary amine-impregnated activated carbon: Integrated experimental and first-principles approach, Chem. Eng. J. 373 (2019) 1003–1011.
[13] J.L. Kovach, History of radioiodine control, in: Proceedings of the 25th DOE/NRC Nuclear Air Cleaning and Treatment Conference, 1998, pp. 304–319.
[14] F. Kepák, Removal of gaseous fission products by adsorption, J. Radioanal. Nucl. Chem. 142 (1990) 215–230.
[15] C.Y. Yin, M.K. Aroua, W.M.A.W. Daud, Review of modifications of activated carbon for enhancing contaminant uptakes from aqueous solutions, Sep. Purif. Technol. 52 (3) (2007) 403–415.
[16] C.M. González-García, J.F. González, S. Román, Removal efficiency of radioactive methyl iodide on TEDA-impregnated activated carbons, Fuel Process. Technol. 92 (2011) 247–252.
[17] Ro, et al., United States Patent 5792720. Method and apparatus for manufacturing TEDA– impregnated active carbon in fluidized bed type absorbing tower by generating TEDA vapor by means of hot air. US5792720A – Method and apparatus for manufacturing TEDA-impregnated active carbon in fluidized bed type absorbing tower by generating TEDA vapor by means of hot air –, Google Patents.
[18] N. Mori, N. Kamishima, Radioactive iodine adsorbent and radioactive iodine removal apparatus, US Patent 9044737 (2011) https://patents.justia.com/patent/9044737.
[19] "Iodine trap of activated carbons (Acticarb Nuclear, Camfil)," Camfil. https://www.camfil.com/fr-fr/produits/filtres-moleculaires/filtres-compacts-type-cellule/acticarb/acticarb-_-39856.
[20] K.S. Sing, D. Everett, R.A. Haul, L. Moscou, R. Pierotti, J. Rouquerol, T. Siemieniewska, Reporting Physisorption Data for Gas/Solid Systems with Special Reference to the Determination of Surface Area and Porosity, Pure Appl. Chem. 57 (1985) 603–619.
[21] S. Brunauer, P.H. Emmet, E. Teller, Adsorption of Gases in Multimolecular Layers, J. Am. Soc. 60 (1938) 309–319.
[22] G. Horvath, K. Kawazoe, Method for the Calculation of Effective Pore Size Distribution in Molecular Sieve Carbon, J. Chem. Eng. Jpn. 16 (6) (1983) 470–475.
[23] E.P. Barrett, L.G. Joyner, P.P. Halenda, The Determination of Pore Volume and Area Distributions in Porous Substances. I. Computations from Nitrogen Isotherms, J. Am. Chem. Soc. 73 (1951) 373–380.
[24] H. Estrade-Szwarckopf, XPS Photoemission in Carbonaceous Materials: A "Defect" Peak beside the Graphitic Asymmetric Peak, Carbon 42 (2004) 1713–1721.
[25] E.F. Sheka, Y.A. Golubev, N.A. Popova, Amorphous state of sp2 solid carbon, Fuller. Nanotub. Carbon Nanostruct. 29 (2) (2021) 107–113.
[26] F. Rodríguez-Reinoso, M. Molina-Sabio, Textural and chemical characterization of microporous carbons, Adv. Colloid Interface Sci. 76–77 (1998) 271–294.
[27] M.E. Schuster, M. Hävecker, R. Arrigo, R. Blume, M. Knauer, N.P. Ivleva, D.S. Su, R. Niessner, R. Schlögl, Surface Sensitive Study To Determine the Reactivity of Soot with the Focus on the European Emission Standards IV and VI, J. Phys. Chem. A 115 (12) (2011) 2568–2580.
[28] J.G. Wihlelm, "Iodine filters in nuclear power stations." Report KFK 2449, Karlsruhe, Germany, 1977.
[29] Y. Hayashi, G. Yu, M.M. Rahman, K.M. Krishna, T. Soga, T. Jimbo, M. Umeno, Spectroscopic properties of nitrogen doped hydrogenated amorphous carbon films grown by radio frequency plasma-enhanced chemical vapor deposition, J. Appl. Phys. 89 (2011) 7924–7931.
[30] https://srdata.nist.gov/xps/main_search_menu.aspx
[31] M. Chebbi, B. Azambre, L. Cantrel, M. Huvé, T. Albiol, Influence of structural, textural and chemical parameters of silver zeolites on the retention of methyl iodide, Microprous Mesoporous Mater. 244 (2017) 137–150.
[32] S. Brunauer, L.S. Deming, W.S. Demming, E. Teller, J. Amer, On a Theory of the van der Waals Adsorption of Gases, Chem. Soc. 62 (1940) 1723–1732.
[33] M. Guisnet, F. Ribeiro, Les Zéolithes un Nanomonde au Service de la Catalyse, EDP Sciences, 2006.
[34] C.G. Doll, C.M. Sorensen, T.W. Bowyer, J.I. Friese, J.C. Hayes, E. Hoffmann, R. Kephart, Abatement of xenon and iodine emissions from medical isotope production facilities, J. Environ. Radioact. 130 (2014) 33–43.
[35] J. Laine, S. Yunes, Effect of the Preparation Method on the Pore Size Distribution of Activated Carbon from Coconut Shell, Carbon 30 (1992) 601–604.
[36] S.W. Park, W.K. Lee, H. Moon, Adsorption and desorption of gaseous methyl iodide in a triethylenediamine- impregnated activated carbon bed, Sep. Technol. 3 (1993) 133–142.
[37] K. Ho, D. Park, M.K. Park, C.H. Lee, Adsorption mechanism of methyl iodide by triethylenediamine and quinuclidine-impregnated activated carbons at extremely low pressures, Chem. Eng. J. 396 (2020) 125215.
[38] A. International, Standard Test Method for Nuclear-Grade Activated Carbon, ASTM, 2014 D3803-91(2014).
[39] D.M. Ruthven, Principles of Adsorption and Adsorption Processes, John Wiley and Sons, New-York, 1984.
[40] R.H. Perry, D.W. Green, Perry's Chemical Engineers' Handbook, 7th éd., McGraw-Hill, New-York, 1997.
[41] Z. Yu, J. Deschamps, L. Hamon, P.K. Prabhakaran, P. Pré, Modeling hydrogen diffusion in hybrid activated carbon-MIL-101(Cr) considering temperature variations and surface loading changes, Microporous Mesoporous Mater. 248 (2017) 72–83.
[42] E. Glueckauf, J.I. Coates, Theory of chromatography; the influence of incomplete equilibrium on the front boundary of chromatograms and on the effectiveness of separation, J. Chem. Soc. 0 (1947) 1315–1321.
[43] C. Landaverde-Alvarado, A.J. Morris, S.M. Martin, Gas sorption and kinetics of CO2 sorption and transport in a polymorphic microporous MOF with open Zn (II) coordination sites, J. CO2 Util. 19 (2017) 40–48.
[44] T. Qiu, Y. Zeng, C. Ye, H. Tian, Adsorption Thermodynamics and Kinetics of p-Xylene on Activated Carbon, J. Chem. Eng. Data 57 (2012) 1551–1556.
[45] J. Gan, N.E. Megonnell, S.R. Yates, Adsorption and catalytic decomposition of

methyl bromideand methyl iodide on activated carbons, Atmos. Environ. 35 (2001) 941–947.
[46] M.R. Armstrong, B. Shan, Z. Cheng, D. Wang, J. Liu, B. Mu, Adsorption and diffusion of carbon dioxide on the metal-organic framework CuBTB, Chem. Eng. Surf. 167 (2017) 10–17.
[47] A.J. Fletcher, E.J. Cussen, D. Bradshaw, M.J. Rosseinsky, K.M. Thomas, Adsorption of Gases and Vapors on Nanoporous Ni2(4,4'-Bipyridine)3(NO3)4 Metal–Organic Framework Materials Templated with Methanol and Ethanol: Structural Effects in Adsorption Kinetics, J. Am. Chem. Soc. 126 (2004) 9750–9759.
[48] S.W. Park, H.S. Park, W.K. Lee, H. Moon, Effect of water vapor on adsorption of methyl iodide to triethylenediamine-impregnated activated carbons, Sep. Technol. 5 (1995) 35–44.
[49] G.Il. Park, I.T. Kim, J.K. Lee, S.K. Ryu, J.H. Kim, Effect of Temperature on the Adsorption and Desorption Characteristics of Methyl Iodide over TEDA-Impregnated Activated Carbon, Carbon lett. 2 (2001) 9–14.
[50] M.C. Almazán-Almazán, F.J. López-Domingo, M. Domingo-García, A. Léonard, M. Pérez-Mendoza, J.P. Pirard, F.J. López-Garzón, S. Blacher, Influence of carbon xerogel textural properties on the dynamic adsorption of methyl iodide, Chem. Eng. J. 173 (2011) 19–28.
[51] L. Langmuir, The adsorption of gases on plane surfaces of glass, mica and platinum, J. Am. Chem. Soc. 40 (1918) 1361–1403.
[52] H.K. Lee, G.I. Park, J. Kor, Adsorption characteristics of elemental iodine and methyl iodide on base and TEDA impregnated Carbon, Nucl. Soc. 28 (1996) 44–55.
[53] edited by M.M. Dubinin, D.A. Cadenhead, J.E. Danielli, M.D. Rosenberg, Progress in Surface and Membrane Science, 9 Academic Press, New York, 1975. edited by.
[54] R.G. Pearson, Absolute Electronegativity and Hardness: Application to Inorganic Chemistry, Inorg. Chem. 27 (4) (1988) 734–740.
[55] B. Azambre, M. Chebbi, Evaluation of Silver Zeolites Sorbents Toward Their Ability to Promote Stable CH3I Storage as AgI Precipitates, ACS Appl. Mater. Interfaces 9 (30) (2017) 25194–25203.
[56] M. Nakamura, T. Ohba, P. Branton, H. Kanoh, K. Kaneko, Equilibration-time and pore-width dependent hysteresis of water adsorption isotherm on hydrophobic microporous carbons, Carbon 48 (2010) 305–312.
[57] D.D. Do, H.D. Do, A model for water adsorption in activated carbon, Carbon 38 (2000) 767–773.